Enhancement of Acidic HER by Fe Doped CoP with Bimetallic Synergy

Yuanfeng Gao, Hong Lv(✉), Yongwen Sun, Han Yao, Ding Hu, and Cunman Zhang

Clean Energy Automotive Engineering Center, School of Automotive Studies, Tongji University, Shanghai, China
lvhong@tongji.edu.cn

Abstract. Compared to single metal site catalysis, the bimetallic synergistic strategy can exploit the complementary ability of different active sites for active species uptake and desorption to develop excellent catalysts. Pure phase metal phosphides are a disadvantage as a promising electrocatalyst for platinum-free hydrogen precipitation with either too strong or too weak adsorption of hydrogen. Here, synthetic Fe-doped CoP particles anchored with MWCNTs, which exhibited excellent catalytic performance for HER, required an overpotential of 123 mV to reach 10 mA cm^{-2}, with a Tafel slope of 58.8 mV dec^{-1}. It was found experimentally that Fe doping improved the conductivity of the catalyst regulated the electronic structure of CoP, and optimized the overall hydrogen adsorption energy of the catalyst. The difference in hydrogen adsorption strength of Fe, Co is used to break the symmetry constraint of single active center and improve the intrinsic activity of the catalyst, a strategy that can be used to guide the preparation of inexpensive and high performance catalysts.

Keywords: Fe-doped CoP · HER · Synergistic strategy

1 Introduction

Traditional fossil fuel resources are dwindling, and their combustion produces large amounts of pollutants and greenhouse gases, which have a serious impact on the environment. Therefore, developing clean energy is a major challenge facing the world today. Hydrogen (H_2), with a calorific value of ≈282 kJ mol^{-1}, is a clean and sustainable energy source and an ideal substitute for fossil fuels [1–3]. The combustion of hydrogen does not produce greenhouse gases such as carbon dioxide, which can effectively reduce air pollution and greenhouse gas emissions [4]. Electrocatalytic hydrogen evolution can produce clean hydrogen through the reaction of splitting water into hydrogen and oxygen, which can be used as a clean energy medium [5].

The hydrogen evolution reaction (HER) to produce hydrogen gas from cheap electrons generated by renewable energy is a central issue in the manufacture of zero-carbon and carbon-neutral energy carriers [6]. Currently hindering the development of HER is the lack of catalysts with high performance and excellent stability. The current study

H. Sun et al. (Eds.): WHTC 2023, SPPHY 393, pp. 465–474, 2024.
https://doi.org/10.1007/978-981-99-8631-6_45

shows that noble metal-based catalysts (Pt, Ru, Ir, etc.) exhibit the best catalytic performance in electrochemical water splitting [7–10]. However, the scarcity of global reserves and high price of precious metals limit their wide application.

Attempts have been made to replace noble metal-based electrocatalysts with transition metals. Non-noble metal alloys, transition metal sulphides [11–15], phosphides [16–22], carbides [1, 23], and nitrides [24–28] have demonstrated their potential as efficient and durable HER catalysts. Among them, CoP is the most promising substitute due to its high catalytic activity and durability [29–31]. Although the morphology of phosphide has been tuned to obtain a large number of active sites, unfortunately, its performance and durability are still not ideal compared with the noble metal Pt.

In order to improve the intrinsic activity of metal phosphide HER, doping with metallic elements becomes a promising approach Charge transfer between external atoms and the host occurs, and the electronic structure is adjusted to enhance the kinetic process of HER. Most of the current studies focus on the doping of noble metal atoms to improve HER performance, and there is a lack of research on transition metal element doping. In addition, the limited enhancement of HER performance of transition metal-doped phosphides has hindered the research of cheap and durable CoP catalysts.

Fe^{3+} is more acidic among transition metals and can serve as lewis acid sites. Specifically, Fe^{3+} with higher acidity than Co^{2+} can pull electrons from the neighboring Co-P bond, reducing the electronic energy associated with Co^{2+} oxidation and causing a positive change in the corresponding Co redox [6]. Therefore, we hypothesize that the enhanced HER activity can be attributed to the introduction of more acidic substituents into more electron-rich Fe centers through inductive effects. The electron-rich Fe provides electrons to protons, which are easily trapped and form H_{ad} active material. After giving a certain voltage, enough Had is accumulated and then transferred to the electron-deficient Co sites, where Co is beneficial for proton desorption. Both of them have different tasks and synergistically improve the performance of HER. This bimetallic synergistic effect is helpful to guide us to discover more potential catalysts.

2 Experiment Section

2.1 Chemicals

Iron chloride hexahydrate ($FeCl_3 \cdot 6H_2O$), cobalt chloride hexahydrate ($CoCl_2 \cdot 6H_2O$), Sodium hypophosphite ($NaH_2PO_2 \cdot H_2O$), methanol (CH_3OH) and hexamethylenetetramine (HMT) were purchased from Sigma-Aldrich and directly used without further purification. Ultrapure deionized water (DI, 18.4 MΩ cm^{-1}) was used in all experiments. MWCNTs were purchased from Tanfeng Tech. Inc (China). Cabon paper HCP020P were purchased from Shanghai Hesen Electric Co., Ltd (China).

2.2 Preparation of $Co_{1-x}Fe_xLDH$/MWCNTs

In a typical synthesis process of $Co_{0.75}Fe_{0.25}LDH$/MWCNTs, the total moles of Co and Fe are 2. The MWCNTs (100 mg) was dispersed into the water of 70 mL to form a dispersion solution under continuous ultrasonication. Subsequently, 0.5 mmol iron chloride

hexahydrate ($FeCl_3 \cdot 6H_2O$), 1.5 mmol cobalt chloride hexahydrate ($CoCl_2 \cdot 6H_2O$), and 0.875 mmol hexamethylenetetramine (HMT) were added into the above solution under vigorous stirring. The solution was refluxed at 100 °C for 5 h in an oil bath, and then the precipitates were collected by centrifugation for several times with water and alcohol. The samples were dried at 60 °C overnight to obtain $Co_{0.75}Fe_{0.25}$LDH/MWCNTs. For comparison, the bulky $Co_{0.75}Fe_{0.25}$LDH samples without MWCNTs were also obtained under the same conditions. Other CoFeLDH/MWCNTs, prepared by adjusting the proportion of Fe.

2.3 Preparation of $Co_{1-x}Fe_xP$/MWCNTs

To prepare the $Co_{0.75}Fe_{0.25}$P/MWCNTs, a low temperature phosphidation method was employed here. In details, 300 mg of $NaH_2PO_2 \cdot H_2O$ and as-synthesized $Co_{0.75}Fe_{0.25}$P/MWCNTs were placed in the quartz boats individually, and then placed in two separate positions within the tube furnace. The furnace was heated up to 300 °C with a temperature ramping rate of 5 °C/min and kept at 300 °C for two hour under an N_2 flow of 100 sccm.

2.4 Electrochemical Measurements

The catalyst ink was prepared by dispersing 4 mg of various catalysts into 1 mL of the mixed solvent containing water, ethanol and 5% Nafion with a volumetric ratio of 768:200:32. For the preparation of the catalytic electrodes, 10 μL of the catalyst ink was loaded onto a carbon paper (CP) electrode. A CHI760E electrochemical workstation was used to conduct all the electrochemical tests, with an CP as the working electrode, a graphite rod as the counter electrode, a Hg/Hg_2SO_4 electrode as the reference electrode, and 0.5 M H_2SO_4 as the electrolyte. The CV result is shown in Fig. S1. Before the electrochemical test, $E(RHE) = E(Hg/Hg_2SO_4) + 0.71$ V for 0.5 M H_2SO_4 electrolyte.

3 Results and Discussion

The morphology of the catalysts was characterized by SEM and TEM. The SEM images (Fig. 1a) showed that the nanoparticles were grown on the surface of the MWCNTs and the surface-grown catalysts encapsulated the MWCNTs to form a core-shell structure. This structure may provide more active sites for the HER reaction and is thought to improve the catalytic performance. As shown in Fig. 1b, the lattice spacings of $Co_{0.75}Fe_{0.25}$P/MWCNTs of 0.243, 0.238 and 0.283 nm correspond to [111], [201] and [002] crystal planes, respectively, which are very close to the lattice spacings of the corresponding crystal planes of $(CoFe)P_2$. The high-angle annular dark field image (HAADF) map shows that the nanoparticles are uniformly dispersed on the surface of MWCNTs (Fig. 1c), which also indicates that electrons can interact with the catalyst nanoparticles rapidly through the MWCNTs channels. The STEM-EDX map shows the same distribution area of Fe, Co and P elements, which proves that the products are uniformly distributed on the surface of MWCNTs, indicating that Fe doped CoP was successfully synthesized (Fig. 1d).

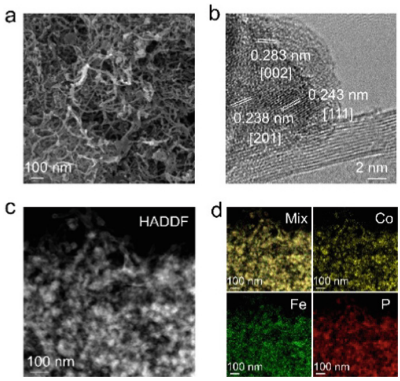

Fig. 1. (**a**) SEM and (**b**) HR-TEM image of $Co_{0.75}Fe_{0.25}P$/MWCNTs. (**c**) HAADF-STEM images and the corresponding. (**d**) STEM-EDX of $Co_{0.75}Fe_{0.25}P$/MWCNTs.

The surface composition and chemical properties of $Co_{0.75}Fe_{0.25}P$/MWCNTs were investigated by x-ray photoelectron spectroscopy (XPS). As shown in Fig. 2a, the Co 2p XPS spectra of $Co_{0.75}Fe_{0.25}P$/MWCNTs had characteristic peaks at 781.8 and 797.9 eV, which were assigned to Co^{3+} [32]. The Co 2p XPS spectra had characteristic peaks at 783.7 and 799.2 eV, which were assigned to Co^{2+}, and the other peak positions were assigned to satellite peaks. The characteristic peaks of Fe 2p XPS spectra (Fig. 2b) in $Co_{0.75}Fe_{0.25}P$/MWCNTs at 712.4 and 726.3 eV, which are attributed to Fe^{3+}. The characteristic peaks of Fe 2p XPS spectra at 710.2 and 724.5 eV, which are assigned to Fe^{2+}, and other peak positions are attributed to satellite peaks [33]. The Co 2p and Fe 2p XPS spectra of $Co_{0.75}Fe_{0.25}P$/MWCNTs indicate that the acidic Fe^{3+} pulls electrons out of the Co site, leading to a change in the electronic structure of the catalyst. The characteristic peaks of the O 2p XPS spectra (Fig. 2c) in $Co_{0.75}Fe_{0.25}P$/MWCNTs at 531.8 and 533.3 eV, respectively attributed to surface oxygen and exogenous oxygen. The lattice oxygen is not found in the O 2p XPS spectra, which indicates that no metal phosphate is formed [34]. P 2p XPS spectra at 130.1 and 131.2 eV for the low valence P [35] and higher binding energy at 134.3 eV are attributed to PO_4^{3-} or P_2O_5, which is attributed to the oxidation of the surface P element [36].

The HER activity of $Co_{0.75}Fe_{0.25}P$/MWCNTs in 0.5 M H_2SO_4 was determined by linear scanning voltammetry (LSV). For comparison, CoP/MWCNTs, FeP/MWCNTs and 20% Pt/C loaded on carbon paper (CP) substrates were prepared. The LSV (Fig. 3a) showed that $Co_{0.75}Fe_{0.25}P$/MWCNTs had a higher activity towards HER with an overpotential of only 126 mV at 10 mA cm^{-2}, which was significantly smaller than that on CoP/MWCNTs (233 mV) and FeP/MWCNTs (160 mV).

As shown in Fig. 3b, $Co_{0.75}Fe_{0.25}P$/MWCNTs delivered a small Tafel slope of 89.8 mV dec^{-1}, close to that for the commercially available Pt/C catalyst (48.9 mV dec^{-1}), which was lower than CoP/MWCNTs (102 mV dec^{-1}) and FeP/MWCNTs (100 mV dec^{-1}), indicating favorable HER activity. To predict the intrinsic catalytic reaction kinetics of the sample, the Tafel slope was derived from the corresponding polarization curve using the Tafel formula ($\eta = \mathbf{a} + \mathbf{b} \log \boldsymbol{j}$, where $\boldsymbol{b}$ is the Tafel slope, and $\boldsymbol{j}$ is the current density). A lower Tafel slope indicates more efficient hydrogen

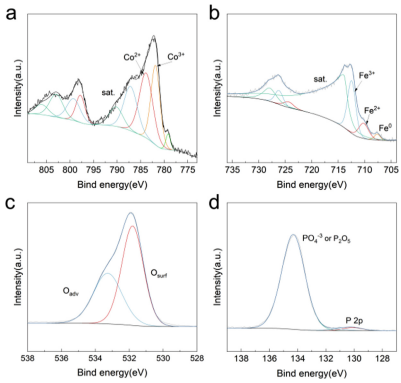

Fig. 2. (**a**) High-resolution XPS spectra of Co 2p, (**b**) Fe 2p, (**c**) O 2p and (**d**) P 2p for $Co_{0.75}Fe_{0.25}P$/MWCNTs.

reaction evolution dynamics, meaning that increasing the same current density requires smaller overpotentials.

It is well known that under a specific set of conditions, the HER mechanism is divided into two steps in acidic solution, which are electrochemical adsorption process (Volmer) and desorption process (Heyrovsky or Tafel). Generally, a Tafel slope of 120 mV dec^{-1} indicates that the Volmer step is the rate-determining step:

$$H^- + e^- + * \rightarrow *H_{ads}$$

This step is followed by either an electrochemical desorption step (Heyrovsky reaction, Tafel slope is 40 mV dec^{-1}) [37],

$$H^- + e^- + * + *H_{ads} \rightarrow H_2 + 2*$$

or a recombination step (Tafel reaction, Tafel slope is 30 mV dec^{-1}) [38, 39],

$$*H_{ads} + *H_{ads} \rightarrow H_2 + 2*$$

The rate-determining step of Pt/C follows the Volmer-Heyrovsky mechanism in 0.5 M H_2SO_4 solution according to the literature. The Tafel slope of CoP/MWCNTs and FeP/MWCNTs increased to 102 and 100 mV dec^{-1}, all of them indicated a tendency to limit the absorption of H^+ on active sites (Volmer Step). The slope of $Co_{0.75}Fe_{0.25}P$/MWCNTs (89.8 mV dec^{-1}) implies that the reaction mechanism is the Volmer-Heyrovsky mechanism in the HER, in which the rate-determining step is the desorption process and the reaction kinetics is optimized. Analysis of the overpotential and Tafel shows that Fe has a large effect on HER performance. In Fig. 3c, the practical H_2 yield is basically agreement with the theoretical value, giving a faradaic efficiency of nearly 99% for HER in 0.5 M H_2SO_4. The electrochemical impedance spectrum shows a charge transfer resistance of 7.1 Ω for $Co_{0.75}Fe_{0.25}P$/MWCNTs, which is close to Pt/C (7 Ω) and less than CoP/MWCNTs (10.2 Ω) and FeP/MWCNTs (8.9 Ω). This also indicates that Fe doping modulates the electronic structure of the catalysts, making the charge transport more efficient.

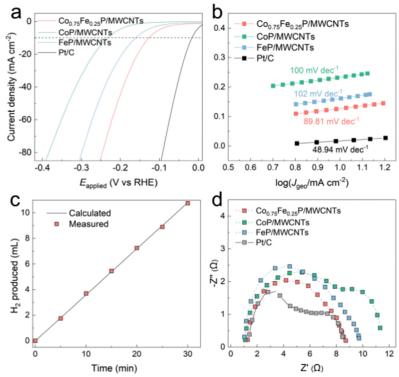

Fig. 3. (**a**) SEM and (**b**) HR-TEM image of $Co_{0.75}Fe_{0.25}P$/MWCNTs. (**c**) HAADF-STEM images and the corresponding (**d**) STEM-EDX of $Co_{0.75}Fe_{0.25}P$/MWCNTs. (**a**) HER-LSV curves of $Co_{0.75}Fe_{0.25}P$/MWCNTs, CoP/MWCNTs, FeP/MWCNTs and Pt/C. (**b**) Tafel plots of different samples. (**c**) Faraday efficiency of HER for $Co_{0.75}Fe_{0.25}P$/MWCNTs with constant current density of 100 mA cm^{-2}. (**d**) Nyquist plots for $Co_{0.75}Fe_{0.25}P$/MWCNTs, CoP/MWCNTs, FeP/MWCNTs and Pt/C.

The electrochemical double layer capacitance (C_{dl}) was determined by cyclic voltammetry (CV). As shown in Fig. 4a, b and c, $Co_{0.75}Fe_{0.25}P$/MWCNTs exhibited a larger C_{dl} of 3.2 mF cm^{-2} in contrast to CoP/MWCNTs (2.2 mF cm^{-2}) and FeP/MWCNTs (2.1 mF cm^{-2}). The larger electrochemically active surface area of $Co_{0.75}Fe_{0.25}P$/MWCNTs indicates that the Fe doped CoP is a dual active site.

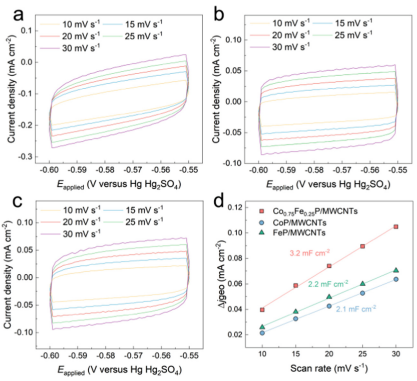

Fig. 4. CV curves at the non-Faradic region of (**a**) $Co_{0.75}Fe_{0.25}P$/MWCNTs, (**b**) CoP/MWCNTs and (**c**) FeP/MWCNTs. (**d**) Double-layer capacitance (Cdl) of $Co_{0.75}Fe_{0.25}P$/MWCNTs, CoP/MWCNTs and FeP/MWCNTs.

When evaluating HER electrocatalysts, the TOF value at the overpotential of −0.2 V versus RHE reveal the intrinsic activity of the catalyst. According to the estimated number of active sites, the TOF value (Fig. 5a) of each active site of $Co_{0.75}Fe_{0.25}P$/MWCNTs, CoP/MWCNTs and FeP/MWCNTs in 0.5 M H_2SO_4 was calculated. As shown in

Fig. 5a, the TOF value of $Co_{0.75}Fe_{0.25}P$/MWCNTs (0.18 s^{-1}) was higher than that of CoP/MWCNTs and FeP/MWCNTs, which further indicates the synergistic effect of the bimetallic sites. The ECSA-normalized specific activity (SA) at $\eta = -200$ mV is shown in Fig. 5b. $Co_{0.75}Fe_{0.25}P$/MWCNTs (SA = 556 $\mu A\ cm^{-2}$) offers higher specific activity than the bare CoP/MWCNTs (SA = 386 $\mu A\ cm^{-2}$) and FeP/MWCNTs (SA = 86 $\mu A\ cm^{-2}$), demonstrating the effectiveness of the bimetallic synergy strategy. Furthermore, the mass activity (MA) is calculated at the overpotential (η) of −200 mV (Fig. 5c), and $Co_{0.75}Fe_{0.25}P$/MWCNTs shows higher MA (107 A g^{-1}) than CoP/MWCNTs (MA = 52 A g^{-1}), and FeP/MWCNTs (MA = 11 A g^{-1}). The corresponding specific activity and mass activity of HER at the overpotential of −200 mV were showed in Fig. 5d, which demonstrating the bimetallic synergistic strategy is potentially applicable to the exploration of superior catalysts.

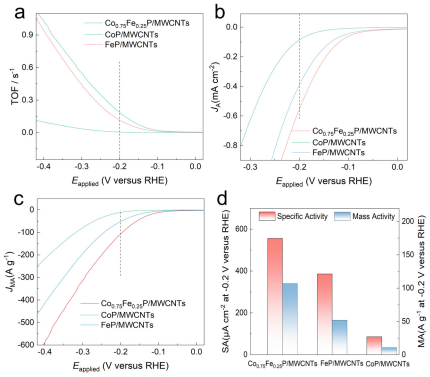

Fig. 5. **a** Turnover Frequency (TOF) plots of $Co_{0.75}Fe_{0.25}P$/MWCNTs, CoP/MWCNTs and FeP/MWCNTs. **b** OER-LSV curves for specific activity, and **c** mass activity of different catalysts. **d** The corresponding specific activity and mass activity of OER at the overpotential of −0.2 V versus RHE.

4 Conclusion

In summary, the $Co_{0.75}Fe_{0.25}P$/MWCNTs catalyst with heterogeneous structure and strong metal carrier interaction was synthesized by hydrothermal method. A series of physical characterization and chemical experiments showed that the unique bimetallic synergy of the $Co_{0.75}Fe_{0.25}P$/MWCNTs composite and the SMSI between the nano-nanoparticles and the MWCNTs substrate give the material superior electronic conductivity, abundant active sites and stable structure, which are the fundamental reasons for its high electrocatalytic HER activity and stability. The $Co_{0.75}Fe_{0.25}P$/MWCNTs catalysts have an overpotential of only 126 mV at a current density of 10 mA cm^{-2} in 0.5 M H_2SO_4 solution and TOF values as high as 0.18 s^{-1} at an overpotential of −200 mV. The bimetallic synergy can provide a promising strategy for the design of superior HER catalysts. Provides a promising strategy for the design of superior HER catalysts.

References

1. Li, J., et al.: Mechanistic insights on ternary $Ni_{2-x}Co_xP$ for hydrogen evolution and their hybrids with graphene as highly efficient and robust catalysts for overall water splitting. Adv. Func. Mater. **26**, 6785–6796 (2016). https://doi.org/10.1002/adfm.201601420
2. Dresselhaus, M.S., Thomas, I.L.: Alternative energy technologies. Nature **414**, 332–337 (2001). https://doi.org/10.1038/35104599
3. Holladay, J.D., Hu, J., King, D.L., Wang, Y.: An overview of hydrogen production technologies. Catal. Today **139**, 244–260 (2009). https://doi.org/10.1016/j.cattod.2008.08.039
4. Seh, Z.W., Kibsgaard, J., Dickens, C.F., Chorkendorff, I., Nørskov, J.K., Jaramillo, T.F.: Combining theory and experiment in electrocatalysis: Insights into materials design. Science **355**, eaad4998 (2017). https://doi.org/10.1126/science.aad4998
5. Turner, J.A.: Sustainable hydrogen production. Science **305**, 972–974 (2004). https://doi.org/10.1126/science.1103197
6. Yuan, S., et al.: Tunable metal hydroxide–organic frameworks for catalysing oxygen evolution. Nat. Mater. **21**, 673–680 (2022). https://doi.org/10.1038/s41563-022-01199-0
7. Liu, D., et al.: Atomically dispersed platinum supported on curved carbon supports for efficient electrocatalytic hydrogen evolution. Nat. Energy **4**, 512–518 (2019). https://doi.org/10.1038/s41560-019-0402-6
8. Alinezhad, A., et al.: Direct growth of highly strained Pt islands on branched ni nanoparticles for improved hydrogen evolution reaction activity. J. Am. Chem. Soc. **141**, 16202–16207 (2019). https://doi.org/10.1021/jacs.9b07659
9. Tiwari, J.N., et al.: Multicomponent electrocatalyst with ultralow Pt loading and high hydrogen evolution activity. Nat. Energy **3**, 773–782 (2018). https://doi.org/10.1038/s41560-018-0209-x
10. Liang, C., et al.: Exceptional performance of hierarchical ni–fe oxyhydroxide@NiFe alloy nanowire array electrocatalysts for large current density water splitting. Energy Environ. Sci. **13**, 86–95 (2020). https://doi.org/10.1039/C9EE02388G
11. Bonde, J., Moses, P.G., Jaramillo, T.F., Nørskov, J.K., Chorkendorff, I.: Hydrogen evolution on nano-particulate transition metal sulfides. Faraday Discuss. **140**, 219–231 (2009). https://doi.org/10.1039/B803857K
12. Sun, Y., Huang, C., Shen, J., Zhong, Y., Ning, J., Hu, Y.: One-step construction of a transition-metal surface decorated with metal sulfide nanoparticles: a high-efficiency electrocatalyst for hydrogen generation. J. Colloid Interface Sci. **558**, 1–8 (2020). https://doi.org/10.1016/j.jcis.2019.09.090
13. Guo, Y., et al.: Nanoarchitectonics for transition-metal-sulfide-based electrocatalysts for water splitting. Adv. Mater. **31**, 1807134 (2019). https://doi.org/10.1002/adma.201807134
14. Li, H., et al.: Systematic design of superaerophobic nanotube-array electrode comprised of transition-metal sulfides for overall water splitting. Nat. Commun. **9**, 2452 (2018). https://doi.org/10.1038/s41467-018-04888-0
15. Huang, C., et al.: Electrolyzer with hierarchical transition metal sulfide and phosphide towards overall water splitting. Mater. Today Phys. **11**, 100162 (2019). https://doi.org/10.1016/j.mtphys.2019.100162
16. Are metal chalcogenides: Nitrides, and phosphides oxygen evolution catalysts or bifunctional catalysts? ACS Energy Lett. **2**, 1937–1938 (2017). https://doi.org/10.1021/acsenergylett.7b00679
17. Tan, Y., et al.: Versatile nanoporous bimetallic phosphides towards electrochemical water splitting. Energy Environ. Sci. **9**, 2257–2261 (2016). https://doi.org/10.1039/C6EE01109H
18. Yan, L., et al.: Metal-organic frameworks derived nanotube of nickel–cobalt bimetal phosphides as highly efficient electrocatalysts for overall water splitting. Adv. Funct. Mater. **27**, 1703455 (2017). https://doi.org/10.1002/adfm.201703455

19. Feng, Y., Yu, X.-Y., Paik, U.: Nickel cobalt phosphides quasi-hollow nanocubes as an efficient electrocatalyst for hydrogen evolution in alkaline solution. Chem. Commun. **52**, 1633–1636 (2016). https://doi.org/10.1039/C5CC08991C
20. Ha, D.-H., et al.: Activity and stability of cobalt phosphides for hydrogen evolution upon water splitting. Nano Energy **29**, 37–45 (2016). https://doi.org/10.1016/j.nanoen.2016.04.034
21. Du, H., Kong, R.-M., Guo, X., Qu, F., Li, J.: Recent progress in transition metal phosphides with enhanced electrocatalysis for hydrogen evolution. Nanoscale **10**, 21617–21624 (2018). https://doi.org/10.1039/C8NR07891B
22. Lu, S.-S., et al.: Tungsten-doped ni–co phosphides with multiple catalytic sites as efficient electrocatalysts for overall water splitting. J. Mater. Chem. A **7**, 16859–16866 (2019). https://doi.org/10.1039/C9TA03944A
23. McKone, J.R., Sadtler, B.F., Werlang, C.A., Lewis, N.S., Gray, H.B.: Ni–mo nanopowders for efficient electrochemical hydrogen evolution. ACS Catal. **3**, 166–169 (2013). https://doi.org/10.1021/cs300691m
24. Xie, J., Xie, Y.: Transition metal nitrides for electrocatalytic energy conversion: opportunities and challenges. Chemistry **22**, 3588–3598 (2016). https://doi.org/10.1002/chem.201501120
25. Abghoui, Y., Skúlason, E.: Hydrogen evolution reaction catalyzed by transition-metal nitrides. J. Phys. Chem. C **121**, 24036–24045 (2017). https://doi.org/10.1021/acs.jpcc.7b06811
26. Yu, L., et al.: A universal synthesis strategy to make metal nitride electrocatalysts for hydrogen evolution reaction. J. Mater. Chem. A **7**, 19728–19732 (2019). https://doi.org/10.1039/C9TA05455C
27. Balogun, M.-S., Huang, Y., Qiu, W., Yang, H., Ji, H., Tong, Y.: Updates on the development of nanostructured transition metal nitrides for electrochemical energy storage and water splitting. Mater. Today **20**, 425–451 (2017). https://doi.org/10.1016/j.mattod.2017.03.019
28. Jin, H., et al.: Molten salt-directed catalytic synthesis of 2d layered transition-metal nitrides for efficient hydrogen evolution. Chem **6**, 2382–2394 (2020). https://doi.org/10.1016/j.chempr.2020.06.037
29. Zhang, H., Maijenburg, A.W., Li, X., Schweizer, S.L., Wehrspohn, R.B.: Bifunctional heterostructured transition metal phosphides for efficient electrochemical water splitting. Adv. Func. Mater. **30**, 2003261 (2020). https://doi.org/10.1002/adfm.202003261
30. Chu, S., et al.: Holey Ni-Cu phosphide nanosheets as a highly efficient and stable electrocatalyst for hydrogen evolution. Appl. Catal. B **243**, 537–545 (2019). https://doi.org/10.1016/j.apcatb.2018.10.063
31. Zhu, J., Hu, L., Zhao, P., Lee, L.Y.S., Wong, K.-Y.: Recent advances in electrocatalytic hydrogen evolution using nanoparticles. Chem. Rev. **120**, 851–918 (2020). https://doi.org/10.1021/acs.chemrev.9b00248
32. Xiao, Z., et al.: Operando identification of the dynamic behavior of oxygen vacancy-rich Co_3O_4 for oxygen evolution reaction. J. Am. Chem. Soc. **142**, 12087–12095 (2020). https://doi.org/10.1021/jacs.0c00257
33. Huang, G., Zhao, L., Yuan, S., Li, N., Jing, S.: Iron doped mesoporous cobalt phosphide with optimized electronic structure for enhanced hydrogen evolution. Int. J. Hydrogen Energy **47**, 14767–14776 (2022). https://doi.org/10.1016/j.ijhydene.2022.02.223
34. Zhai, Y., Ren, X., Sun, Y., Li, D., Wang, B., Liu, S.: Synergistic effect of multiple vacancies to induce lattice oxygen redox in NiFe-layered double hydroxide oer catalysts. Appl. Catal. B **323**, 122091 (2023). https://doi.org/10.1016/j.apcatb.2022.122091
35. Tang, C., et al.: Fe-doped cop nanoarray: A monolithic multifunctional catalyst for highly efficient hydrogen generation. Adv. Mater. **29**, 1602441 (2017). https://doi.org/10.1002/adma.201602441
36. Guan, C., et al.: Hollow Mo-doped CoP nanoarrays for efficient overall water splitting. Nano Energy **48**, 73–80 (2018). https://doi.org/10.1016/j.nanoen.2018.03.034

37. Dinh, C.-T., et al.: Multi-site electrocatalysts for hydrogen evolution in neutral media by destabilization of water molecules. Nat. Energy **4**, 107–114 (2019). https://doi.org/10.1038/s41560-018-0296-8
38. Men, Y., Li, P., Zhou, J., Cheng, G., Chen, S., Luo, W.: Tailoring the electronic structure of Co_2P by N doping for boosting hydrogen evolution reaction at all pH values. ACS Catal. **9**, 3744–3752 (2019). https://doi.org/10.1021/acscatal.9b00407
39. Men, Y., Li, P., Yang, F., Cheng, G., Chen, S., Luo, W.: Nitrogen-doped CoP as robust electrocatalyst for high-efficiency pH-universal hydrogen evolution reaction. Appl. Catal. B **253**, 21–27 (2019). https://doi.org/10.1016/j.apcatb.2019.04.038